Available online at www.sciencedirect.com
ScienceDirect
International Journal of Heat and Mass Transfer 51 (2008) 5426–5442
International Journal of HEAT and MASS TRANSFER
www.elsevier.com/locate/ijhmt

High heat flux flow boiling in silicon multi-microchannels – Part III: Saturated critical heat flux of R236fa and two-phase pressure drops

Bruno Agostini [a], Rémi Revellin [b], John Richard Thome [a,*], Matteo Fabbri [c], Bruno Michel [c], Daniele Calmi [c], Urs Kloter [c]

[a] Heat and Mass Transfer Laboratory (LTCM), l'Ecole Polytechnique Fédérale de Lausanne (EPFL), CH-1015 Lausanne, Switzerland
[b] Centre de Thermique de Lyon (CETHIL) UMR 5008 CNRS-INSA-Univ. Lyon 1 Bât. Sadi Carnot, INSA-Lyon, F-69621 Villeurbanne Cedex, France
[c] IBM Zürich Research Laboratory, Säumerstrasse 4/Postfach, CH-8803 Rüschlikon, Switzerland

Received 14 April 2007
Available online 17 July 2008

Abstract

New experimental critical heat flux results for saturated boiling conditions have been obtained for R236fa flowing in a silicon multi-microchannel heat sink composed of 67 parallel channels, 223 μm wide, 680 μm high and with 80 μm thick fins separating the channels. The microchannel length was 20 mm. The footprint critical heat fluxes measured varied from 112 to 250 W/cm^2 and the wall critical heat fluxes from 21.9 to 52.2 W/cm^2 for mass velocities from 276 to 992 kg/m^{2}s. When increasing the mass velocity, the wall critical heat flux was observed to increase. The inlet saturation temperatures ($20.31 \leqslant T_{sat,in} \leqslant 34.27$ °C) and the inlet subcoolings ($0.4 \leqslant \Delta T_{sub} \leqslant 15.3$ K) were found to have a negligible influence on the saturated CHF. The best methods for predicting the data were those of Wojtan et al. [L. Wojtan, R. Revellin, J. R. Thome, Investigation of critical heat flux in single, uniformly heated microchannels, Exp. Therm. Fluid Sci. 30 (2006) 765–774] and Revellin and Thome [R. Revellin, J. R. Thome, A theoretical model for the prediction of the critical heat flux in heated microchannels, Int. J. Heat Mass Transfer 50 (in press)]. They both predict the experimental CHF results with a mean absolute error of around 9%. Using the critical vapour quality, an annular-to-dryout transition is also proposed as a limit in a diabatic microscale flow pattern map. Pressure drop measurements were measured and analysed, showing that the homogeneous model could correctly predict the observed trends.

Keywords: Critical heat flux; Microchannel; Flow boiling; Refrigerant; Chip cooling

1. Introduction

In the micro-electronics industry, mini and microchannel cooling technologies have attracted considerable attention in recent years because of the substantial increase of heat flux to dissipate (Kandlikar et al. [3] refers to microchannels as channels having an hydraulic diameter less than 0.2 mm and minichannels between 0.2 and 3 mm, while for Kew and Cornwell [4] the transition occurs for a confinement number around 0.5). Traditional approaches such as natural or forced convection using air show very poor performances at high imposed heat flux. Dissipation of high heat flux while maintaining microprocessor operating temperatures below 85 °C can be achieved using flow boiling in microchannels. However, one of the limiting operating conditions with flow boiling is the critical heat flux (CHF) or burnout. CHF, which refers to the replacement of liquid being in contact with the heated surface with a vapour blanket, is characterized by a dramatic drop of the surface heat transfer coefficient. The resulting effect is a rapid increase of the surface temperature and possible failure of the cooled device. CHF may occur in subcooled

* Corresponding author. Tel.: +41 21 693 5981; fax: +41 21 693 5960.
E-mail address: john.thome@epfl.ch (J.R. Thome).

0017-9310/$ - see front matter © 2008 Elsevier Ltd. All rights reserved.
doi:10.1016/j.ijheatmasstransfer.2008.03.005

Nomenclature

A'	parameter of Bowring's [13] correlation
C'	parameter of Bowring's [13] correlation
C_f	fanning friction factor
c_p	specific heat capacity (J/kg K)
CHF	critical heat flux (W/m^2)
D	diameter (m)
$D_h = 4WH/(2W+2H)$	hydraulic diameter m
$D_e = 4WH/(W+2H)$	heated equivalent diameter (m)
$D_G = \sqrt{(4HW/\pi)}$	mass velocity equivalent diameter (m)
Δh_{in}	inlet enthalpy of subcooling (J/kg)
f	friction factor
g	acceleration of gravity (m/s^2)
G	mass velocity (kg/m^2 s)
h	specific enthalpy (J/kg)
h_{lv}	latent heat of vaporization (J/kg)
k	thermal conductivity (W/m K)
K	empirical inlet subcooling parameter of Katto and Ohno [10]
L	length (m)
MAE	Mean absolute error $= \frac{100}{N}\sum_1^N \lvert\frac{\text{predicted}-\text{experimental}}{\text{experimental}}\rvert$ (%)
MRE	Mean relative error $= \frac{100}{N}\sum_1^N (\frac{\text{predicted}-\text{experimental}}{\text{experimental}})$ (%)
n	exponent of Y in Shah's [11,12] correlation
p	pressure (Pa)
q	heat flux (W/m^2)
$q_{CHF,sub}$	CHF for subcooled conditions (W/m^2)
q_{CHF}	saturated CHF of Katto and Ohno [10] (W/m^2)
r	radius of the vapour core (m)
R	internal radius of the tube (m)
Re	Reynolds number
T	temperature (°C)
u	velocity (m/s)
W	channel width (m)
We_D	diameter based Weber number
We_L	channel length based Weber number
x	vapour quality
Y	Shah's [11,12] correlating parameter

Greek symbols

$\Delta\delta_i$	height of the interfacial waves (μm)
Δp	pressure drop (kPa)
δ	film thickness (μm)
γ	equivalent two-phase pressure drop factor
ξ	singular pressure loss coefficient
μ	dynamic viscosity (Pa s)
ω	pressure drop ratio
ρ	density (kg/m^3)
σ	surface tension (N/m)

Subscripts

b	base
CHF	critical heat flux
crit	critical
h	hydraulic
i	interfacial
in	inlet
l	liquid
min	minimum
out	outlet
sat	saturation
sub	subcooling
TP	two-phase
v	vapour
w	wall

as well as in saturated boiling conditions. In subcooled CHF, the bulk temperature at the channel outlet is subcooled and the thermodynamic equilibrium vapour quality is lower than zero. These are the typical conditions for high inlet subcoolings and relatively short channels compared to their hydraulic diameters. In saturated CHF, the thermodynamic equilibrium vapour quality at the channel outlet is greater or equal to zero but less than one. This is typically encountered at low inlet subcoolings and in channels with a large length to diameter ratio.

CHF is an important parameter to study and understand in order to cool electronic chips at safe operating conditions. CHF in conventional channels has been extensively studied in the last decades because of the development of nuclear reactors. Only a few studies have been carried out on CHF in mini and microchannels and none to our knowledge with new low pressure refrigerants such as R236fa. This study is thus devoted to the collection of new experimental results on CHF for R236fa flowing in multi-microchannel heat sinks. A comparison with the existing relevant prediction methods is also carried out to determine the best prediction method.

A second important aspect of micro-evaporator design for cooling of micro-electronics is the pressure drop and its corresponding energy consumption. As a new technology, pointing immediately towards a "green" solution is particularly imperative today. Concerning pressure drops during flow boiling in microchannels, a recent literature study by Ribatski et al. [5] demonstrated that the homogeneous model was one of the best methods for their predicting two-phase pressure drops. However, a real cooling system includes both inlet and outlet manifolds, which will participate in the total pressure drop. The relative contributions of these different parts of the system must be estimated in order to be able to minimize the pressure drop of the system, size the pump and estimate its energy consumption. Accordingly, this study will present total pressure drop data 'across the test section including the inlet

and outlet manifolds, and will analyse their respective contributions to the total.

2. Existing CHF predicting methods

Critical heat flux correlations have first been developed for single tubes. One of the most widely quoted empirical methods developed for predicting saturated CHF in a single channel is Katto and Ohno [6] correlation. For no liquid subcooling, they correlated CHF with

$$\frac{q_{\mathrm{CHF}}}{Gh_{\mathrm{lv}}} = \text{function}\left(\frac{\rho_{\mathrm{l}}}{\rho_{\mathrm{v}}}, \frac{\sigma\rho_{\mathrm{l}}}{G^2 \cdot L}, \frac{L}{D_{\mathrm{h}}}\right), \tag{1}$$

where the appropriate correlating function is chosen depending on the channels' geometry and fluid properties. For most regimes, they found a linear rise in CHF with increasing liquid subcooling. Therefore, subcooling was taken into account by the following equation:

$$q_{\mathrm{CHF,sub}} = q_{\mathrm{CHF}}\left(1 + K\frac{\Delta h_{\mathrm{in}}}{h_{\mathrm{lv}}}\right). \tag{2}$$

To ascertain the applicability of the above correlation to fluids other than water, they conducted the following experiments:

- R12 for $D_{\mathrm{h}} = 3.0$ and 5.0 mm, $L/D_{\mathrm{h}} = 200$ and 333, $\rho_{\mathrm{v}}/\rho_{\mathrm{l}} = 0.109$-0. 306 and $G = 1100$–8800 kg/m^{2}s in Katto and Yokoya [7];
- R12 for $D_{\mathrm{h}} = 5.0$ mm, $L/D_{\mathrm{h}} = 50$, $\rho_{\mathrm{v}}/\rho_{\mathrm{l}} = 0.109$–0. 306 and $G = 700$–7000 kg/m^2 s in [8].
- Liquid helium for $D_{\mathrm{h}} = 1.0$ mm, $L/D_{\mathrm{h}} = 25$–200, $\rho_{\mathrm{v}}/\rho_{\mathrm{l}} = 0.409$ and $G = 10.5$–108 kg/m^2 s in [9].

Hence, for refrigerants this method is applicable only down to about 3.0 mm diameter channels. Katto [10] also proposed a general correlation for predicting CHF of forced convective boiling in uniformly heated rectangular channels fed with subcooled liquid. They concluded by saying that the CHF is nearly equal to the CHF of forced convective boiling on heated plane surfaces in a parallel flow. Their correlation is given by Eq. (2) with different expressions for q_{CHF} and K.

The correlation of Shah [11,12] is also a well-known method for predicting the critical heat flux during upflow in uniformly heated vertical tubes. The correlation was developed with a database that included 23 fluids (water, cryogenic fluids, chemicals and liquid metals), tube diameters from 0.315 to 37.5 mm and tube lengths from 1.3 to 940 tube diameters. These data were taken from 62 independent sources. The correlation is written as

$$\frac{q_{\mathrm{CHF}}}{Gh_{\mathrm{lv}}} = 0.124\left(\frac{L}{D}\right)^{-0.89}\left(\frac{10^4}{Y}\right)^{n}(1 - x_{\mathrm{in}}) \tag{3}$$

with

$$Y = G^{1.8}D^{0.6}\left(\frac{c_{\mathrm{p}}}{k_{\mathrm{l}}\rho_{\mathrm{l}}^{0.8}g^{0.4}}\right)\left(\frac{\mu_{\mathrm{l}}}{\mu_{\mathrm{v}}}\right)^{0.6}. \tag{4}$$

When $Y \leqslant 10^4$, $n = 0$. When $Y > 10^4$, n is given by one of the following relations:

$$\begin{aligned} Y \leqslant 10^6, \quad & n = \left(\frac{D}{L}\right)^{0.54}, \\ Y > 10^6, \quad & n = \frac{0.12}{(1 - x_{\mathrm{in}})^{0.5}}. \end{aligned} \tag{5}$$

Bowring [13] proposed a general correlation for predicting CHF of water flowing in conventional circular tubes. The form of his correlation is

$$q_{\mathrm{CHF}} = \frac{A' + 0.25DGh_{\mathrm{sub}}}{C' + L}, \tag{6}$$

where q_{CHF} is the critical heat flux in W/m^2 and A' and C' are functions of the geometry and the fluid properties. This method is derived from data covering the following parameter ranges: $0.2 < p_{\mathrm{out}} < 19$ MPa, $2 < D < 45$ mm, $150 < L < 3700$ mm and $136 < G < 18{,}600$ kg/m^2 s.

Zhang et al. [14] compared existing correlations for flow boiling of water with available databases from small diameter tubes ($0.33 < D < 6.22$ mm) and developed a new correlation based on the inlet conditions by doing a parametric analysis of the collected database. Their correlation, which predicts their database with a mean absolute deviation of 16.8% is

$$\begin{aligned} \frac{q_{\mathrm{CHF}}}{Gh_{\mathrm{lv}}} = {} & 0.0352\left[We_{\mathrm{D}} + 0.0119\left(\frac{L}{D}\right)^{2.31}\left(\frac{\rho_{\mathrm{v}}}{\rho_{\mathrm{l}}}\right)^{0.361}\right]^{-0.295} \\ & \times \left(\frac{L}{D}\right)^{-0.311}\left[2.05\left(\frac{\rho_{\mathrm{v}}}{\rho_{\mathrm{l}}}\right)^{0.170} - x_{\mathrm{in}}\right] \end{aligned} \tag{7}$$

with

$$We_{\mathrm{D}} = \frac{G^2 D}{\sigma\rho_{\mathrm{l}}}. \tag{8}$$

Qu and Mudawar [15] compared their 414 data points obtained for water in channels with $D = 1.0$–3.0 mm and $L_{\mathrm{h}}/D = 50$–975 and for R113 with $D = 3.15$ mm and $L_{\mathrm{h}}/D = 40$ to the correlation of Katto and Ohno [10]. They found that this correlation was fairly accurate at predicting saturated CHF in single circular mini-channels. The mean absolute error was 17.3% with most of the data points falling within a ±40% error band.

Wojtan et al. [1] performed a series of tests to measure saturated CHF in 0.509 and 0.790 mm internal diameter microchannel tubes as a function of refrigerant mass velocity, heated length, saturation temperature and inlet liquid subcooling. The refrigerants tested were R134a and R245fa and the heated length of the microchannel was varied from 20 to 70 mm. The results showed a strong dependence of CHF on mass velocity, heated length and microchannel diameter but no measurable influence of liquid subcooling (2–15 K) was observed. The experimental

results were compared to the CHF single-channel correlation of Katto and Ohno [6] and the multichannel correlation of Qu and Mudawar [15], showing that the former predicted their microchannel data better than the second, however with a mean absolute error of 32.8% and with only 41.2% of the data falling within a ±15% error band. The correlation of Qu and Mudawar [15] exhibited the same trends as the CHF data but significantly over-predicted them. Based on their experimental data, a new microscale version of Katto and Ohno [6] correlation for the prediction of CHF during saturated boiling in single microchannels was proposed by Wojtan et al. [1]:

$$\frac{q_{\mathrm{CHF}}}{Gh_{\mathrm{lv}}} = 0.437\left(\frac{\rho_{\mathrm{v}}}{\rho_{\mathrm{l}}}\right)^{0.073} We_{\mathrm{l}}^{-0.24}\left(\frac{L}{D}\right)^{-0.72}. \tag{9}$$

Wojtan et al. [1] observed the occurrence of dryout always to be in the annular flow regime. Through an energy balance based on their CHF correlation, they calculated the critical vapour quality. In a mass velocity versus vapour quality diabatic flow pattern map, they reported the annular-to-dryout transition. Beyond this limit mist flow occurs.

Revellin and Thome [2] proposed a theoretical model for predicting CHF in microchannels. The model is based on the premise that the CHF is reached when local dryout occurs during evaporation in annular flow in a uniformly heated, circular microchannel. It is assumed in this model that the mechanism of CHF occurs when the centerline to trough interfacial wave height ($\Delta\delta_i$) on the annular liquid film becomes equal to the average liquid film thickness (δ) without waves, so that the interfacial waves are large enough to have their trough in contact with the wall and thus trigger local dryout and CHF. This situation always occurs for $x < 1$. The hydrodynamic model includes the conservation of mass and momentum and an energy balance with the wall. The entrainment of liquid in the gas core and any conduction effects in the wall are neglected. This model can predict the thickness of the annular liquid film δ in a one dimensional finite volume model. Based on the slip ratio and the Kelvin–Helmoltz critical wavelength (assuming the film thickness to be proportional to the critical wavelength of the interfacial waves), the wave height is predicted as follows in [2]:

$$\Delta\delta_i = 0.15R\left(\frac{u_{\mathrm{v}}}{u_{\mathrm{l}}}\right)^{-3/7}\left(\frac{(\rho_{\mathrm{l}}-\rho_{\mathrm{v}})gR^2}{\sigma}\right)^{-1/7}. \tag{10}$$

The heat flux is determined by iterating until the film thickness is equal to the height of the interfacial waves ($\delta = \Delta\delta_i$). When this is satisfied anywhere along the microchannel, CHF is reached. The empirical parameters of Eq. (10) were determined with a database including three different fluids (R134a, R245fa and R113), three different diameters (0.5, 0.8 and 3.15 mm) from two different laboratories [1,15].

With the increasing interest for micro-electronic cooling, multi-channel CHF correlations have been developed. Qu and Mudawar [15] obtained CHF data for water in a microchannel heat sink containing 21 parallel 215 × 821 μm rectangular channels. They found that as CHF was approached, flow instabilities induced vapour backflow into the heat sink's upstream plenum, resulting in mixing vapour with subcooled liquid. The backflow negated the advantages of inlet subcooling, resulting in a CHF virtually independent of inlet subcooling. Their new empirical correlation, adapted Katto and Ohno [10] correlation to their experimental CHF data for water and R113 (R113 data were obtained by Bowers and Mudawar [16]) in mini/microchannel heat sinks, and is written as follows:

$$\frac{q_{\mathrm{CHF}}}{Gh_{\mathrm{lv}}} = 33.43\left(\frac{\rho_{\mathrm{v}}}{\rho_{\mathrm{l}}}\right)^{1.11} We_{\mathrm{L}}^{-0.21}\left(\frac{L}{D_{\mathrm{e}}}\right)^{-0.36} \tag{11}$$

with

$$We_{\mathrm{L}} = \frac{G^2 L}{\sigma\rho_{\mathrm{l}}}. \tag{12}$$

This correlation predicted their experimental data with a mean absolute error of 4%.

Kuan [17] proposed in his thesis new experimental data points for CHF of water and R123 in multi-microchannels. His test section was composed of six parallel microchannels, having a cross sectional area of 1054 × 157 and 1054 × 197 μm. Flow instabilities were reduced using flow restrictions at the inlet of each microchannel. He found that CHF was increasing when increasing mass velocity. He developed a simple model to predict CHF based on the contact angle between the fluid and the wall. This method will not be used here as this value is not generally known. He also proposed a simple dimensional correlation for predicting his CHF data:

$$q_{\mathrm{CHF}} = 0.2305Gh_{\mathrm{lv}}\left(\frac{L}{D_{\mathrm{e}}}\right)^{-0.9056}. \tag{13}$$

Bergles and Kandlikar [18] reviewed the existing studies on critical heat flux in microchannels. They concluded by saying that for the case of parallel multi-channels all the available CHF data were probably taken under unstable conditions so that the critical condition was the result of an upstream compressible volume instability in the parallel channels, namely the Ledinegg instability. As a result, the CHF values are lower than they would be if the channel flow were kept stable by an inlet restriction at the inlet of each channel for instance or if measured in a single channel.

It has been observed in microchannels that dry-out is the triggering mechanism for CHF. Indeed the liquid starts to disappear at some locations along the channels. Then this dry patch can either be periodically rewetted by liquid (cyclic dry-out) thus producing a heat transfer coefficient decreasing with both heat flux and vapour quality but stable with time, or spread over the whole channel rapidly triggering CHF and the associated dramatic wall temperature increase that ultimately leads to the burn out of the tube.

3. Experimental setup and operating conditions

The experimental setup has been described in Part I of this study. The multi-microchannel heat sink is composed of 67 parallel channels, which are 20 mm long, 223 μm wide and 680 μm high with a fin width of 80 μm separating the channels. An orifice (500 × 223 μm) at the inlet of each channel has been created by the inlet plenum in order to inhibit flow instabilities and backflow.

Five RTDs regularly distributed along the microchannels were used to measure the wall temperatures. As saturated CHF is assumed to occur first at the outlet of the microchannels, the RTD closest to the outlet was specially used to detect CHF. The base heat flux q_b is generated with a serpentine multi-layer resistance heater deposited on the lower face of the die with a lithography process to simulate the microprocessor to cool down. The wall heat flux q_w is calculated with the fin efficiency formula for parallel rectangular fins and is detailed in Part I of this article. A difference between the surface temperature and the saturation temperature greater than 70 °C with a temperature runaway indicated the dryout of the wall and thus the corresponding heat flux at this condition yielded the critical heat flux. An example of heat flux (base and wall values) versus wall superheat made by sequential small steps in heat flux to detect critical heat flux is depicted in Fig. 1. This flow boiling curve shows three different trends:

(i) for $q_b < 23$ W/cm^2, $T_{wall} - T_{sat} \propto q$,
(ii) for $23 < q_b < 200$ W/cm^2, $T_{wall} - T_{sat} \propto q^{0.3}$,
(iii) for $q_b > 200$ W/cm^2, $T_{wall} - T_{sat} \propto q^{\infty}$: CHF is reached.

At a certain heat flux (corresponding to the CHF) the surface temperature increases suddenly, inducing a jump of the temperature difference. This curve shows the way CHF is detected. During experiments, the fluid at the inlet was always subcooled or saturated liquid, by consequence the inlet vapour quality was negative or equal to zero.

4. Experimental results

The different experimental conditions and uncertainties for the CHF tests are summarized in Table 1. The 26 CHF data points are presented in Table 2 in tabular form.

Fig. 2 shows the effect of the mass velocity G on the wall critical heat flux $q_{w,\,CHF}$. As observed previously by other authors [1,15,17], the critical heat flux increases with increasing mass velocity. Multiplying the mass velocity by 2, results in a gain of about 70% in CHF. In Fig. 2, different

Table 1
Experimental conditions and uncertainties

	Value	Error
L (mm)	20	±0.02
W (μm)	223	±10
H (μm)	680	±10
D_e (μm)	383	±15.6
G (kg/m^2 s)	276–992.2	±3%
$q_{b,\,CHF}$ (W/cm^2)	112–250	±0.5%
p_{in} (kPa)	203.1–342.7	±1.5
Δp (kPa)	0.3–125	±0.65
$T_{sat,\,out}$ (°C)	23.4–36.4	±1.5
ΔT_{sub} (K)	15.3–0.4	±0.2
x_{out}	0.5283–1.0676	±0.5%

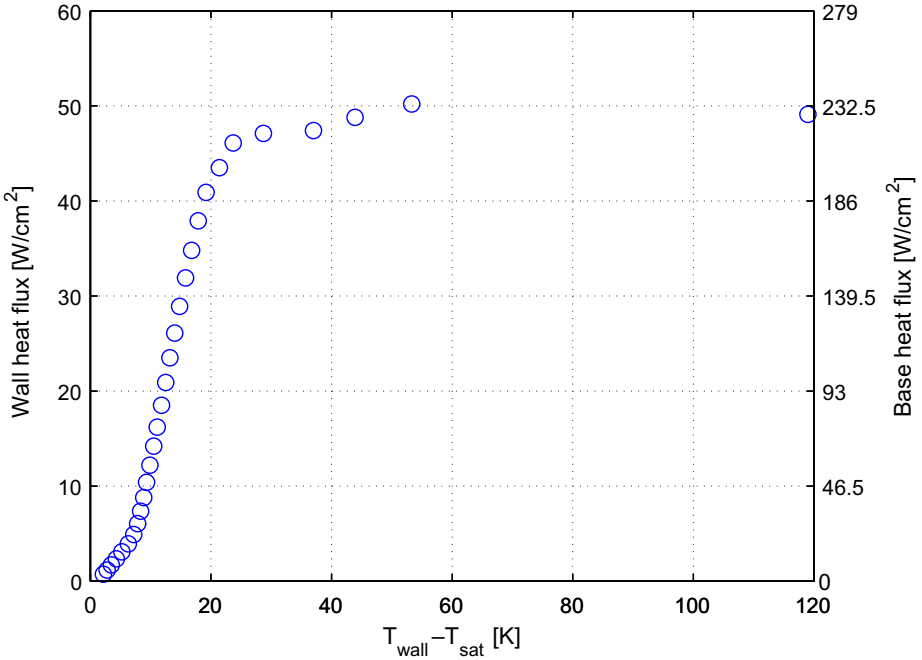

Fig. 1. Convective boiling curve for R236fa, $L = 20$ mm, $W = 223$ μm, $H = 680$ μm, $G = 810$ kg/m^2 s, $\Delta T_{sub} = 0$ K and $T_{sat,in} = 25$ °C. Left scale is the wall heat flux, right scale is the base (footprint) heat flux.

Table 2
Present CHF database

D_e (μm)	$T_{sat,in}$ (°C)	$T_{sat,\ out}$ (°C)	ΔT_{sub} (K)	G (kg/m^2 s)	$q_{b,\ CHF}$ (W/cm^2)	$q_{w,\ CHF}$ (W/cm^2)	x_{in} (dimensionless)	x_{out} (dimensionless)
383	25.74	24.63	0.65	275.79	112.00	21.90	−0.0086	1.0676
383	25.88	23.33	1.50	415.33	145.00	28.96	−0.0118	0.9140
383	25.76	20.61	0.42	548.63	191.00	39.56	−0.0012	0.9241
383	25.80	17.68	0.54	688.35	218.00	45.50	−0.0035	0.8463
383	25.91	14.15	0.62	825.39	235.00	49.40	0.0003	0.7739
383	25.97	25.08	10.52	277.04	114.00	22.34	−0.0906	0.9986
383	25.71	23.16	10.91	425.04	150.00	30.10	−0.0942	0.8435
383	26.05	22.06	10.98	554.42	185.00	37.89	−0.0943	0.7900
383	25.84	19.10	11.03	694.50	220.00	46.07	−0.0936	0.7483
383	25.70	16.25	10.95	829.49	235.00	51.00	−0.0901	0.6766
383	25.83	13.32	11.18	958.69	250.00	52.16	−0.0913	0.6128
383	25.93	25.03	13.98	284.61	113.00	22.12	−0.1191	0.9316
383	25.95	23.74	14.31	431.10	150.00	30.18	−0.1225	0.8022
383	25.86	21.93	14.17	558.16	185.00	37.68	−0.1223	0.7547
383	25.86	19.91	14.97	697.88	214.00	45.97	−0.1280	0.6937
383	25.78	17.69	15.16	833.23	230.00	50.05	−0.1268	0.6172
383	25.77	14.72	15.25	992.20	245.00	49.55	−0.1244	0.5283
383	26.07	24.97	5.15	282.12	114.00	22.32	−0.0444	1.0252
383	26.02	23.56	5.31	407.31	150.00	30.14	−0.0456	0.9289
383	25.96	21.54	5.35	551.13	185.00	37.68	−0.0469	0.8427
383	25.90	18.91	5.39	686.03	215.00	44.32	−0.0417	0.7883
383	25.65	15.00	5.21	823.61	235.00	50.01	−0.0406	0.7312
383	20.31	10.20	4.55	686.03	190.00	39.80	−0.0352	0.7125
383	29.70	24.29	5.40	700.73	215.00	44.80	−0.0467	0.7758
383	34.27	30.42	5.15	696.01	214.00	44.39	−0.0441	0.7816

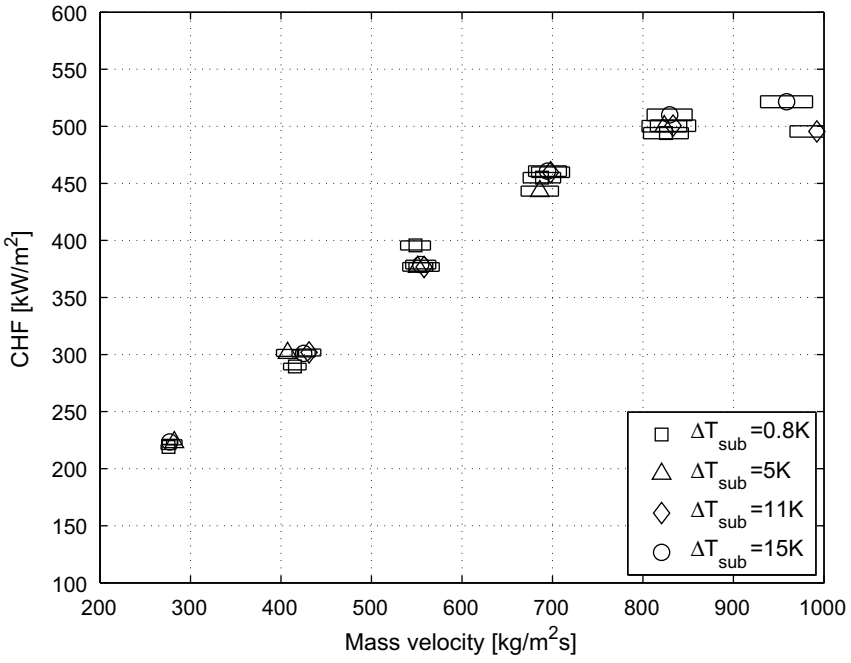

Fig. 2. Experimental wall CHF results as a function of the mass velocity for R236fa, $L = 20$ mm, $W = 223$ μm, $H = 680$ μm, $T_{sat,in} = 26$ °C and ΔT_{sub} between 0 and 15 K. Boxes around symbols represent uncertainties.

inlet subcoolings are presented. All of them follow the same trend with G. For $T_{sat,in} = 26$ °C, the CHF (in terms of the wall heat flux, not the base heat flux) in Fig. 2 increases from 22 to 52 W/cm^2 for a mass velocity increasing from 276 to 959 kg/m^2 s.

The influence of the inlet subcooling is presented in Fig. 2. For the range of ΔT_{sub} considered here, the inlet subcooling has no influence on CHF. The same conclusion had been reached by Wojtan et al. [1] for the same range of ΔT_{sub}. Numerically, Revellin and Thome [2] have shown

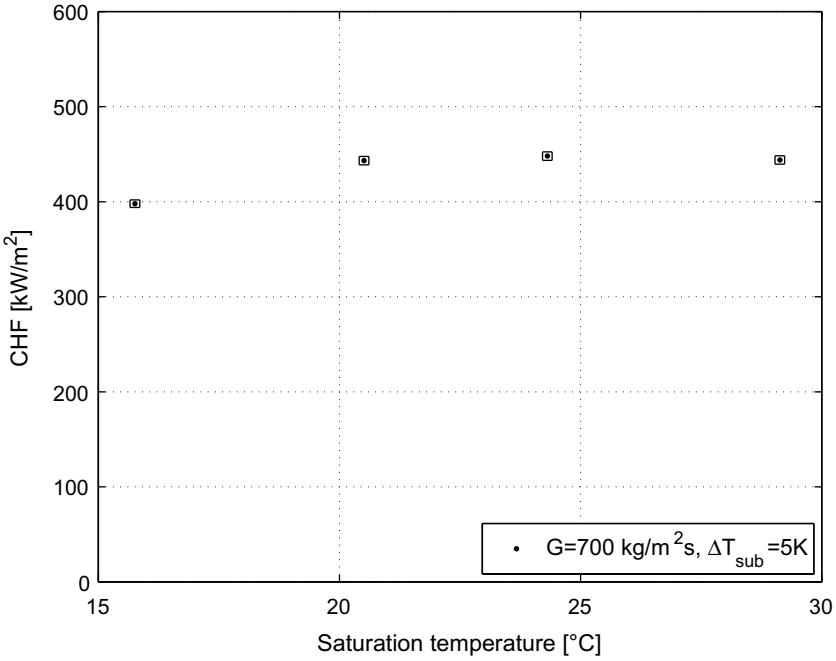

Fig. 3. Experimental wall CHF (q_w) results as a function of the saturation temperature for R236fa, $L = 20$ mm, $W = 223$ μm, $H = 680$ μm, $G = 700$ kg/m^2 s and $\Delta T_{sub} = 5$ K.

that when the inlet subcooling was increased, the CHF was slightly increased by the slight reduction in the effective saturated heated length. The CHF increase was about 15% when the subcooling increased from 0 to 15 K. Even with the presence of the inlet orifices there might be some backflow or recirculation in the rectangular channels (but not in the inlet manifold) that would make the saturated heated length constant even with an increased subcooling.

The effect of the saturation temperature on the wall critical heat flux is depicted in Fig. 3 for a mass velocity of 700 kg/m^2 s and an inlet subcooling ΔT_{sub} equal to 5 K. There is about a 10% effect of the saturation temperature on the CHF for the range $20.31 \leqslant T_{sat,in} \leqslant 34.27$ °C. However, it is difficult to make any general conclusion on the effect of the saturation temperature as the range of temperature variation is small. The footprint (base) CHF is around 210 W/cm^2 in this graph.

As a conclusion, the effects of mass velocity, saturation temperature and inlet subcooling have been studied. As expected, when increasing mass velocity, CHF increases significantly. The saturation temperature and the inlet subcooling were found to have a minor or negligible influence on CHF over the range of parameters studied here.

5. Comparison with existing prediction methods

The present database has been compared to the following methods in the literature for predicting CHF in microchannels:

- Macro-scale methods: Katto and Ohno [6,10], Shah [11,12] and Bowring [13].
- Micro-scale methods: Zhang et al. [14] for water in round microchannels, Qu and Mudawar [15] for water and R113 in rectangular multi-microchannels, Kuan [17] for water and R123 in multi-microchannels, Wojtan et al. [1] for refrigerants R134a and R245fa in round microchannels and Revellin and Thome [2] for different microchannel geometries and fluids.

As the present microchannels are rectangular, an equivalent diameter has to be chosen to characterize its size. This equivalent diameter can take different forms:

- The hydraulic diameter defined as: $D_h = 4WH/(2W + 2H)$.
- The heated equivalent diameter as proposed by Qu and Mudawar [15] and also Katto [10]: $D_e = 4WH/(W + 2H)$ takes into account the heated walls only.
- The mass velocity equivalent diameter is that of a circular channel yielding the same cross sectional area as the rectangular channel, as proposed by Thome et al. [19] in their three-zone model: $D_G = \sqrt{(4HW/\pi)}$.

Here, the heated equivalent diameter was chosen as it better reflects the heat transfer conditions (three sides heated). Comparisons between the experimental results and prediction methods are presented in Table 3. Three statistical tools are used to make the comparison: the percentage of data predicted within a ±20% error band, the mean absolute error (MAE) and the mean relative error (MRE).

Concerning the methods for circular geometries, the correlations of Katto and Ohno [6] (MAE = 15.1%) and Zhang et al. [14] (MAE = 16.5%) give almost the same

Table 3
Comparison of data with prediction methods

Method	% of data within ±20%	MAE (%)	MRE (%)
Katto and Ohno [6] circular channels	80	15.1	12.7
Katto and Ohno [10] rectangular channels	56	18.5	−18.1
Shah [11,12]	0	36.3	−36.3
Bowring [13]	16	25.5	−25.5
Zhang et al. [14]	76	16.5	−16.1
Qu and Mudawar [15]	0	325.3	325.3
Kuan [17]	16	41.1	41.1
Wojtan et al. [1]	100	10.1	−7.1
Revellin and Thome [2]	100	10.1	−9.9

result. The methods capture property effects although they were mainly developed for water. Shah [11,12] macroscale correlation does not predict the data well with a mean absolute error of 36.3%. Since this method is only for macrochannels, the difference observed is not surprising when extrapolating to such small equivalent diameters. The correlation of Bowring [13] also underpredicts the present CHF data with a MRE = −25.5%. The range of pressures and diameters studied here are lower than the pressure and diameter for which the correlation was developed and that may explain the difference. The best methods to predict CHF of R236fa flowing in microchannels are the Wojtan et al. [1] correlation and the Revellin and Thome theoretical model. They both predict 100% of the data within a ±20% error band. The MAE is the same in both cases (10.1%) and the MRE is slightly lower for the correlation, −7.1 against −9.9% for the model. The method of Wojtan et al. [1] tends to better predict the data than the model of Revellin and Thome but the difference is marginal. The correlation is interesting because it is easy to use while the model needs to be solved numerically. However, the model captures apparently the physical phenomena and can be applied to non-uniform heat fluxes and may extrapolate better in terms of fluid properties.

Concerning the methods for rectangular geometries, the correlation of Qu and Mudawar [15] gives the worst overall prediction with a mean absolute error of around 325%. Perhaps this is not surprising because this correlation was developed uniquely for water and R113 whose density ratios (ρ_v/ρ_l) were respectively around 6.3×10^{-4} and 0.005 whereas the present CHF data of R236fa include a density ratio varying from 0.0078 to 0.016. The data of Wojtan et al. [1] for refrigerants were also significantly overpredicted by Qu and Mudawar [15] correlation. Another significant overprediction is observed for the correlation of Kuan [17] (MRE = 41.1%) that was developed for water and R123 in multi-microchannels. The simplistic form of the correlation may explain this difference because the effect of only one fluid property is taken into account. The correlation of Katto [10] for rectangular channels gives a reasonably good agreement (MAE = 15.1%). However, it was seen that for high mass velocities (high CHF) the correlation deviates significantly from the measured results. Generally speaking, the methods for rectangular cross-sections overpredict the data whereas those for circular cross sections underpredict the present CHF results.

In summary, at the present the correlation of Wojtan et al. [1] and the model of Revellin and Thome [2] are the best methods for predicting CHF of R236fa flowing in a rectangular multi-microchannel heat sink with the heated equivalent diameter used as the reference diameter. The CHF values predicted by these two models versus the measured CHF values are shown in Fig. 4.

6. Critical vapour quality

As shown in Wojtan et al. [1] and Revellin and Thome [20], the critical vapour quality defines the annular-to-dryout transition in a diabatic flow pattern map. Beyond this zone, damage from overheating can occur for the device cooled by the microchannels, such as a microprocessor. The critical vapour quality is thus the upper safe operating limit for the exit vapour quality of heat sinks.

Fig. 5 shows the mass velocity versus the critical vapour quality for a saturation temperature of 26 °C and an inlet subcooling of around 11 K. The model of Revellin and Thome is also plotted for comparison with a ±20% error band. The prediction agreement is very good and the trend in the data is also captured. The theoretical critical vapour quality has been determined here using an energy balance as follows, assuming a uniform heat flux along the channel:

$$x_{crit} = \frac{q_{CHF}}{G(h_{lv} + h_{sub})} \frac{4L}{D_e}. \quad (14)$$

It can be concluded that for the conditions considered here, CHF occurs at $x = 1$ for a mass velocity less than 280 kg/m^2 s, namely, when the liquid is totally evaporated as could be seen for the tabular values given in Table 2 with $x_{out} > 1$. When mass velocity increases, critical vapour quality decreases. Extrapolating the critical vapour quality to very high mass velocities may however result in a flow pattern transition. Instead of an annular-to-dryout transition, a bubbly-to-dryout transition would appear as mentioned by Pribyl et al. [21], but this hypothesis should be tested experimentally.

7. Two-phase pressure drop

Two-phase pressure drops are an important design parameter in the design of micro-evaporator cooling systems. The total pressure drop measured in the multi-microchannel test section is composed of three contributions:

(i) The liquid pressure drop, including the singular pressure loss due to the inlet orifices and the frictional pressure drop of any subcooled flow in the microchannels.

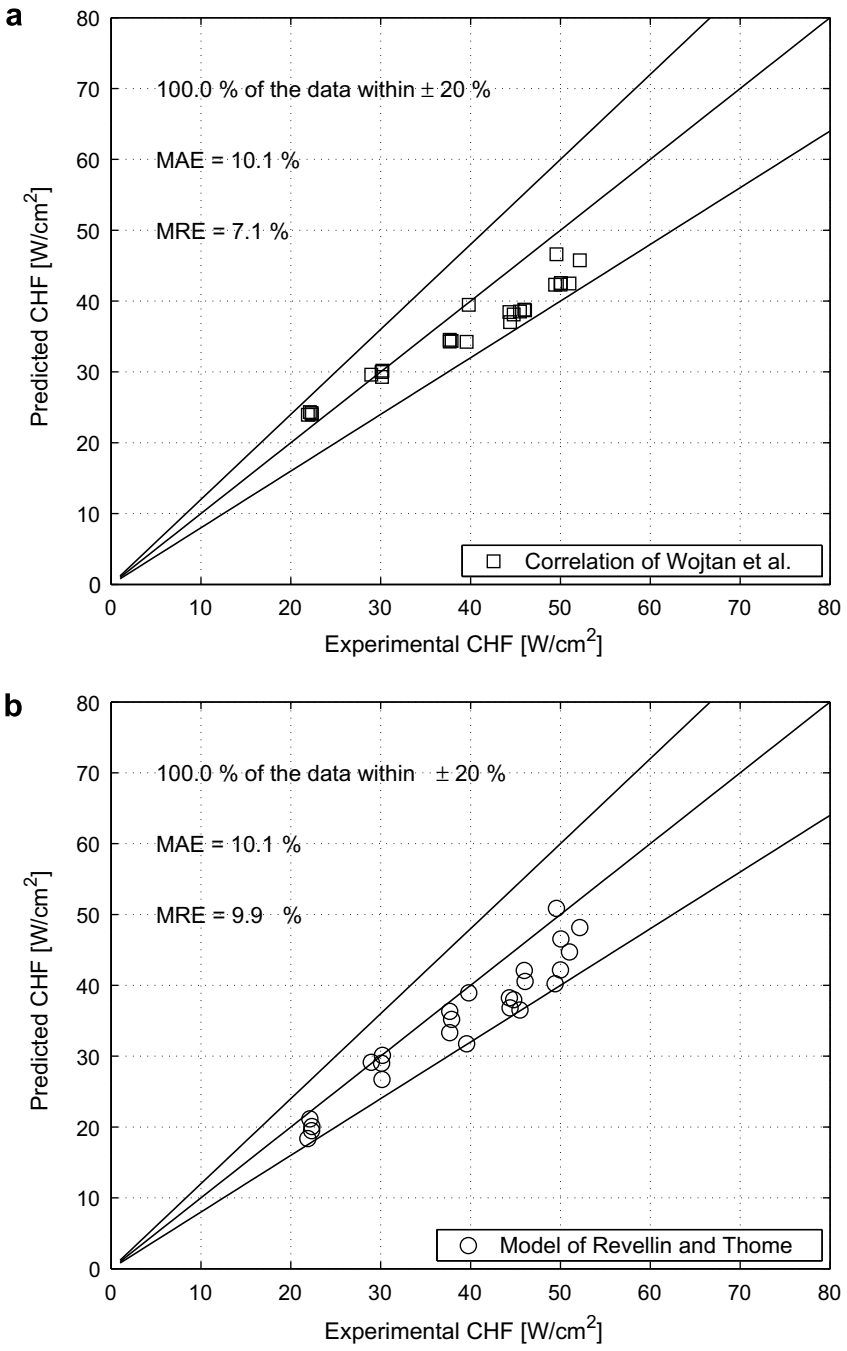

Fig. 4. Comparison between the present experimental CHF data and the Wojtan et al. [1] correlation (a) and the Revellin and Thome [2] prediction method (b).

(ii) The microchannel two-phase pressure drop in the microchannels, including the two-phase frictional pressure drop and the momentum pressure drop.
(iii) The outlet pressure drop, which is composed of a momentum pressure gain due to the sudden enlargement, a pressure loss due to the sharp 90° bend and a singular frictional pressure drop.

The total pressure drop Δp is measured with a differential pressure transducer. The liquid pressure drop Δp_l is calculated from liquid single-phase flow pressure drop measurements (refer to Part I for details). The microchannel two-phase pressure drop Δp_{TP} inside the microchannels is modelled with the homogeneous model, according to the recommendations of Ribatski et al. [5] (see Part I). Finally, the outlet pressure drop is calculated by subtracting the liquid and two-phase contributions from the total measured pressure drop:

$$\Delta p_{out} = \Delta p - \Delta p_L - \Delta p_{TP}. \quad (15)$$

Of course the uncertainty on Δp_{out} can be quite large due to all the terms included in Eq. (15). The error can be as large

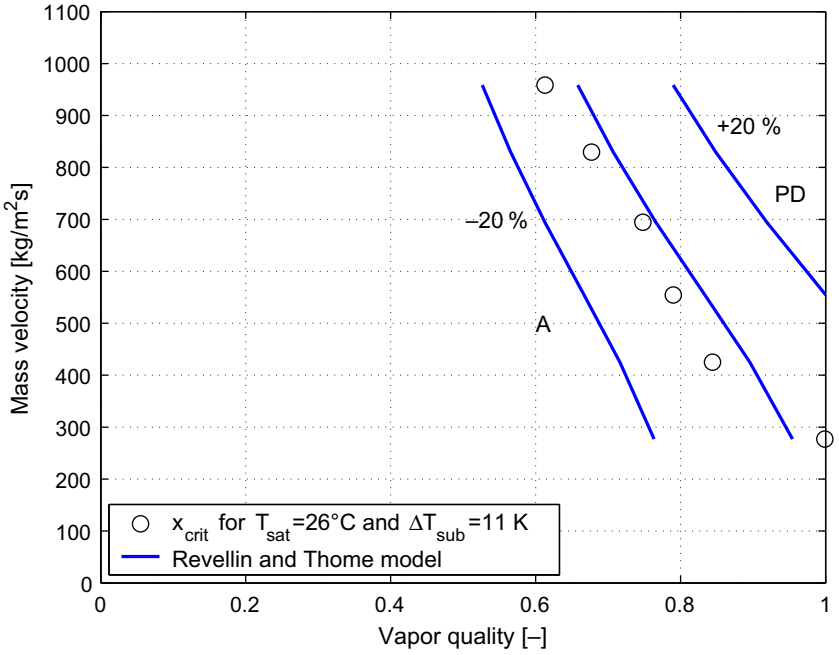

Fig. 5. Comparison between the experimental and the theoretical (from the model of Revellin and Thome) critical vapour quality for R236fa, $L = 20$ mm, $W = 223$ μm, $H = 680$ μm, $T_{sat,in} = 26$ °C and $\Delta T_{sub} = 11$ K. A: Annular regime; PD: Post dryout regime.

as ±100% at the lowest mass velocity and vapour quality (i.e., when the pressure drop is close to zero), but goes down to ±20% at the highest mass velocity and vapour quality.

Fig. 6 shows the total pressure drop versus the outlet vapour quality (i.e., for increasing heat fluxes) for (a) R236fa and (b) R245fa. The convention on all the plots is to represent pressure drops as positive values. Generally speaking, the total pressure drop increases approximately linearly with the outlet vapour quality and increases with mass velocity. The total pressure drop is greater for R245fa than for R236fa at the same pressure, mass velocity and subcooling but this is partly due to the fact that narrower inlet and outlet slits were used with R245fa (200 μm inlet and 500 μm outlet for R245fa against 500 μm inlet and 1000 μm outlet for R236fa).

The regular pressure drop along the channels depends on the fluid properties for a given mass flux, heat flux and channel geometry, which are kept constant between R236fa and R245fa tests. The pressure drops that depend on the slit width are the inlet and outlet pressure drops:

$$\Delta p = \frac{G^2}{2\rho}\xi \propto \frac{M^2}{2\rho D^4}\xi, \tag{16}$$

where ξ usually increases rapidly with decreasing hydraulic diameter so that the singular pressure drop in the inlet and outlet slits are mainly dependent on geometry rather than fluid properties. Thus it can be concluded that the regular pressure drop difference is mainly due to the fluid properties and the singular pressure drop to the geometry change in the manifolds.

Since different inlet and outlet configurations were used for each fluid, it makes most sense to compare the microchannel two-phase pressure drops predicted by the homogeneous model in order to assess the respective pressure drops of R236fa and R245fa. Thus, Fig. 7a and b shows a comparison of the microchannel two-phase pressure drop calculated with the homogeneous model between R236fa and R245fa, at a mass velocity of 1000 kg/m^2 s and a subcooling of 0 K, for an inlet pressure of 282 kPa and a saturation temperature of 25 °C, respectively. In both cases the microchannel two-phase pressure drop of R245fa is higher than that of R236fa, due to its lower vapour density. Indeed, at 282 kPa the vapour density of R236fa is 19 kg/m^3 (saturation temperature is 26 °C) while it is 15.7 kg/m^3 (saturation temperature is 43.5 °C) for R245fa. At a fixed saturation temperature of 25 °C, the vapour density of R236fa is 18.4 kg/m^3 (saturation pressure is 272 kPa) while it is 8.6 kg/m^3 (saturation pressure is 149 kPa) for R245fa. Although it makes more sense physically to compare the pressure drop of the two fluids at the same pressure, for a practical application like computer chip cooling the saturation temperature is fixed typically in the range 20–25 °C so that the comparison should be made at the same saturation temperature. Thus, it can be seen on Fig 7(b) that at 25 °C, the microchannel pressure drop of R245fa is almost 2 times that of R236fa, while the heat transfer coefficients are approximatively the same as seen in Part II. As a consequence, R236fa is the preferred coolant for computer chip cooling applications because of its lower pumping energy consumption.

Fig. 8 shows the total pressure drop versus saturation temperature for R236fa at a mass velocity of 811 kg/m^2 s

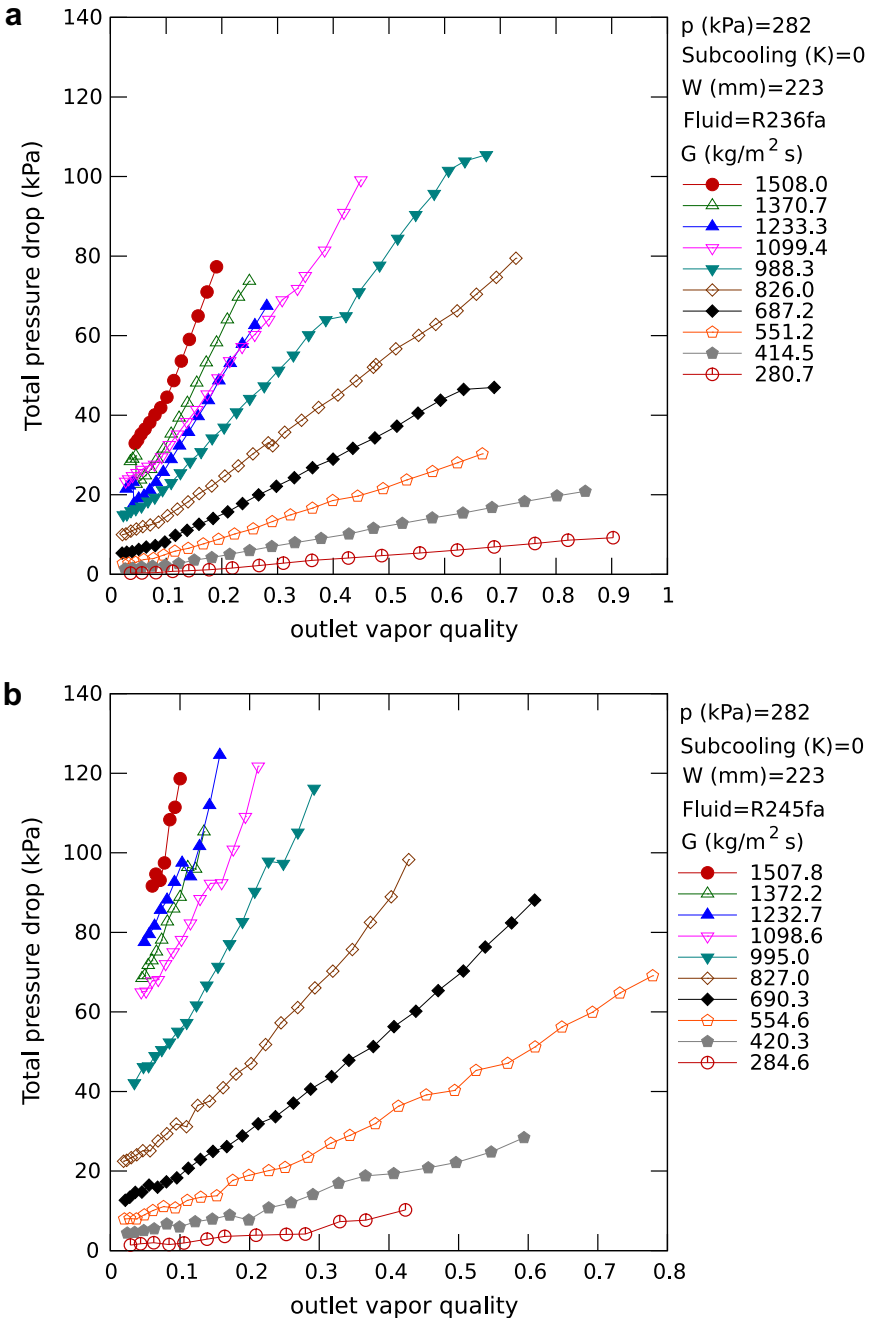

Fig. 6. Total pressure drop versus outlet vapour quality for refrigerant (a) R236fa and (b) R245fa.

and a subcooling of 0 K. As expected, the pressure drop decreases with increasing saturation temperature since the vapour density increases with saturation pressure and temperature.

In order to design and optimize a multi-microchannel cooling system, i.e., trying to achieve the lowest pressure drop for the highest cooling performance, it is useful to calculate the relative contribution of the three components of the total pressure drop. The liquid pressure drop ratio is calculated as

$$\omega_L = \Delta p_L / \Delta p, \tag{17}$$

the microchannel two-phase pressure drop ratio is calculated as

$$\omega_{TP} = \Delta p_{TP} / \Delta p \tag{18}$$

and the outlet pressure drop ratio is calculated as

$$\omega_{out} = \Delta p_{out} / \Delta p. \tag{19}$$

Figs. 9–11 show the liquid, two-phase and outlet pressure drop ratios respectively, for R236fa (a) and R245fa (b). For R236fa, at low vapour quality (<0.1), the total pressure drop is mainly due to the liquid pressure drop. The outlet pressure drop can even be negative at a very low

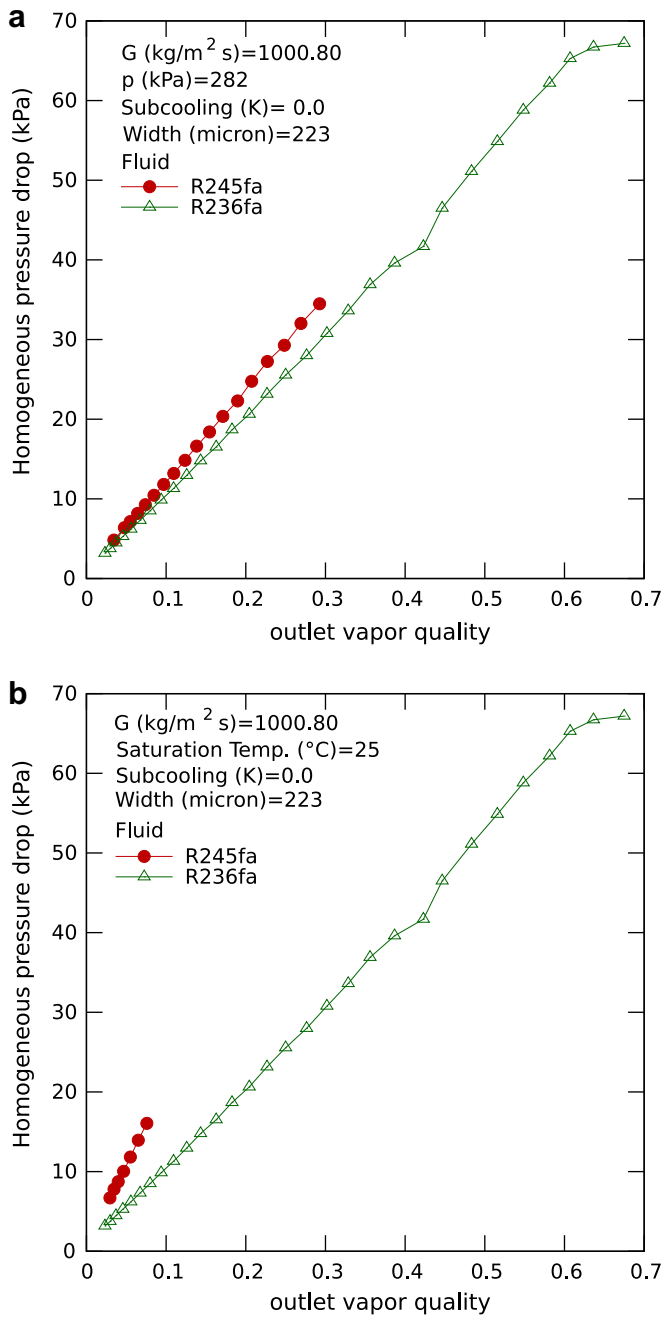

Fig. 7. Comparison of the microchannel two-phase pressure drops for refrigerants R236fa and R245fa: (a) pressure fixed at 282 kPa, (b) saturation temperature fixed at 25 °C.

mass velocity when the recovery in momentum pressure due to the flow area enlargement supersedes the singular pressure loss. However, the liquid pressure drop ratio quickly decreases with increasing vapour quality and the two-phase pressure drop within the microchannels becomes the dominant pressure drop up to a vapour quality of 0.1–0.2. Meanwhile, the outlet pressure drop ratio typically remains constant or even decreases at high mass velocity for R236fa. At higher vapour quality the two-phase pressure drop ratio remains constant or decreases at low mass velocity while the outlet pressure drop ratio increases, but

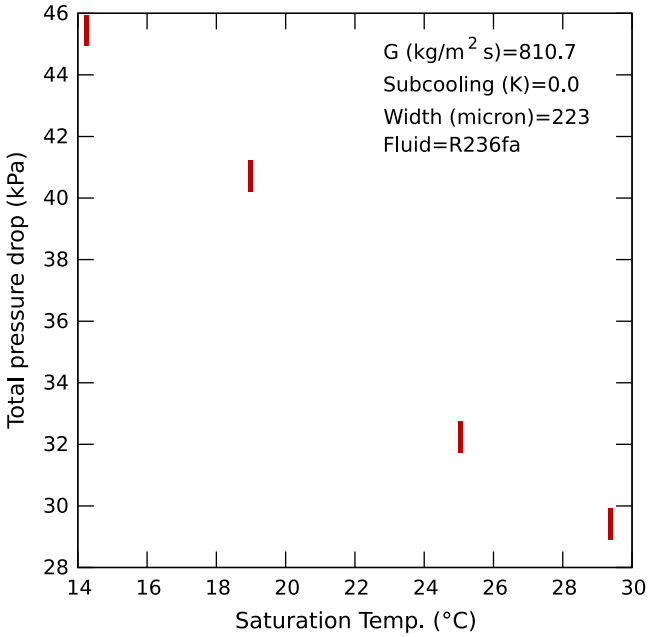

Fig. 8. Influence of saturation temperature on total pressure drop for refrigerant R236fa. The box symbols represent uncertainties in both directions.

the two-phase pressure drop in the microchannels remains the dominant pressure drop contribution.

For R245fa the trends differ depending on mass velocity. For mass velocities between 407 and 815 kg/m^2 s, the behaviour is the same as for R236fa. For higher mass velocities the outlet pressure drop is always the dominant pressure drop contribution but this is mainly due to narrower inlet and outlet slits used with R245fa.

The analysis of these plots is instructive for the design of a two-phase micro-evaporator cooling system. With the present channel geometry, which has not been optimized, a typical flow boiling chip cooling application will run with R236fa at 25 °C saturation temperature, a mass velocity of 1000 kg/m^2 s and an outlet vapour quality of 0.6 for a base heat flux of 200 W/cm^2, yielding a total pressure drop of 100 kPa. Out of these 100 kPa, 10% are attributable to the inlet orifice, 60% to the two-phase flow inside the microchannels and 30% to the outlet manifold, meaning that a lower total pressure drop can be obtained firstly by operating at a lower mass velocity and secondly by a better design of the outlet manifold.

Using the homogeneous model, the total pressure drop can be written as

$$\Delta p = \frac{G^2}{2\rho_L}\left(2\left(\frac{\rho_L}{\rho_v}-1\right)\left(1+\frac{\gamma}{4}\right)x+(\gamma+\xi_{in})\right) \tag{20}$$

with

$$\gamma = 4f_{TP}\frac{L_{TP}}{D_h}+\xi_{out}, \tag{21}$$

$$4f_{TP} = 0.316Re_{TP}^{-0.25}, \tag{22}$$

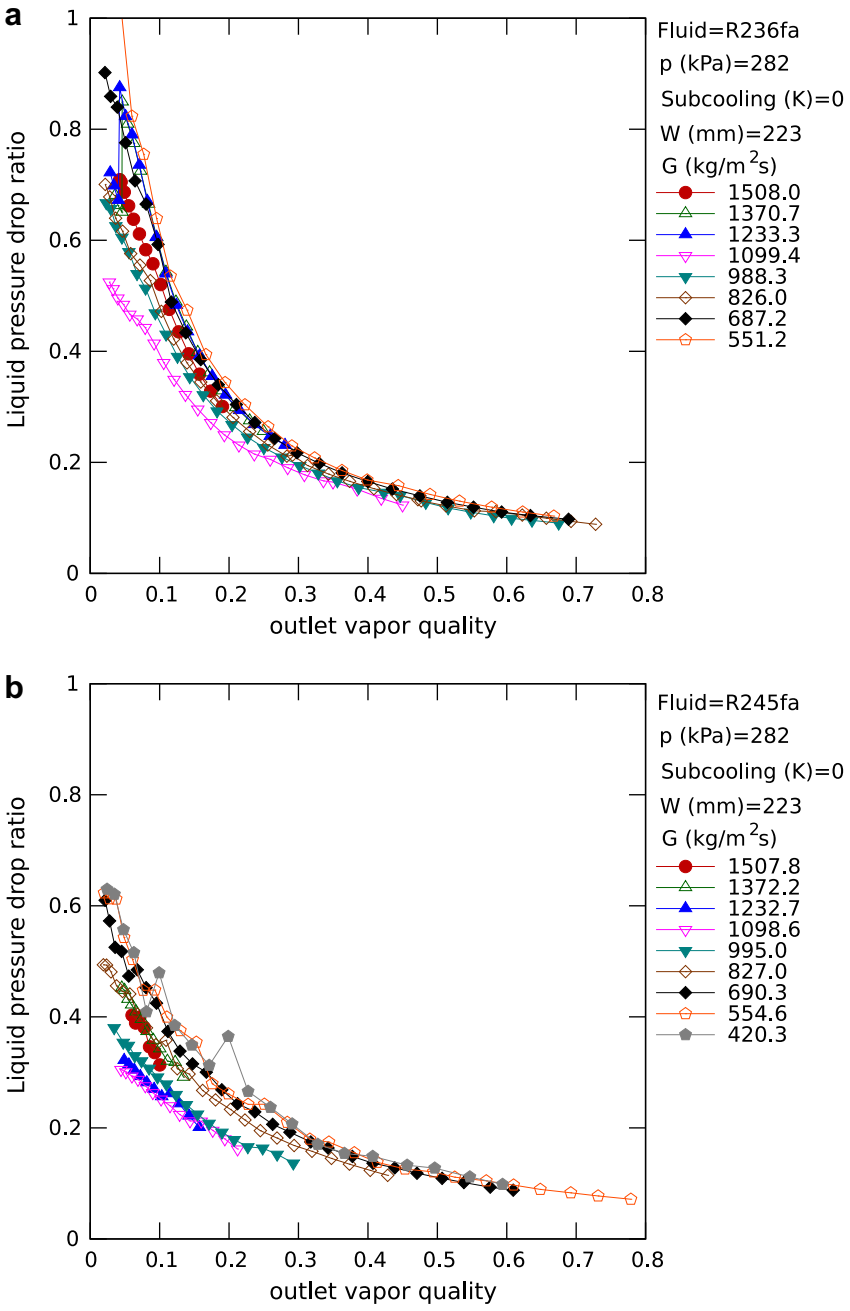

Fig. 9. Inlet pressure drop ratio versus outlet vapour quality for refrigerant R236fa (a) and R245fa (b).

$$Re_{TP} = \frac{GD_h}{\mu_{TP}}, \tag{23}$$

$$\mu_{TP} = (1-x)\mu_L + x\mu_v, \tag{24}$$

where $4f_{TP}$ is the two-phase friction factor calculated as explained in Part I, μ_{TP} is the two-phase viscosity calculated using Ciccitti et al. [22] definition (like in Part I), ξ_{in} is the inlet singular pressure drop coefficient determined from the single-phase flow experiments, ξ_{out} is the outlet singular pressure drop coefficient, which is a constant value unknown at this point and L_{TP} the two-phase flow length. Now, knowing the total pressure drop, ξ_{out} can be estimated, with a least square method yielding $\xi_{out} = 0.7$ for R236fa and $\xi_{out} = 8.4$ for R245fa. These values are very different because the inlet and outlet slit configurations were modified after the R245fa measurements and before the R236fa tests in order to reduce the total pressure drop (otherwise the test facility could not be run for R236fa because of the singular pressure drop would have been too large through the slits for the pump to handle). Furthermore, the pressure change through a sudden expansion is a function not only of geometry but also of the vapour and liquid densities of the fluid.

The values of the two-phase Reynolds number calculated with Eq. (23) range from 300 to 3200, so that theoretically an expression for a laminar flow should be used in

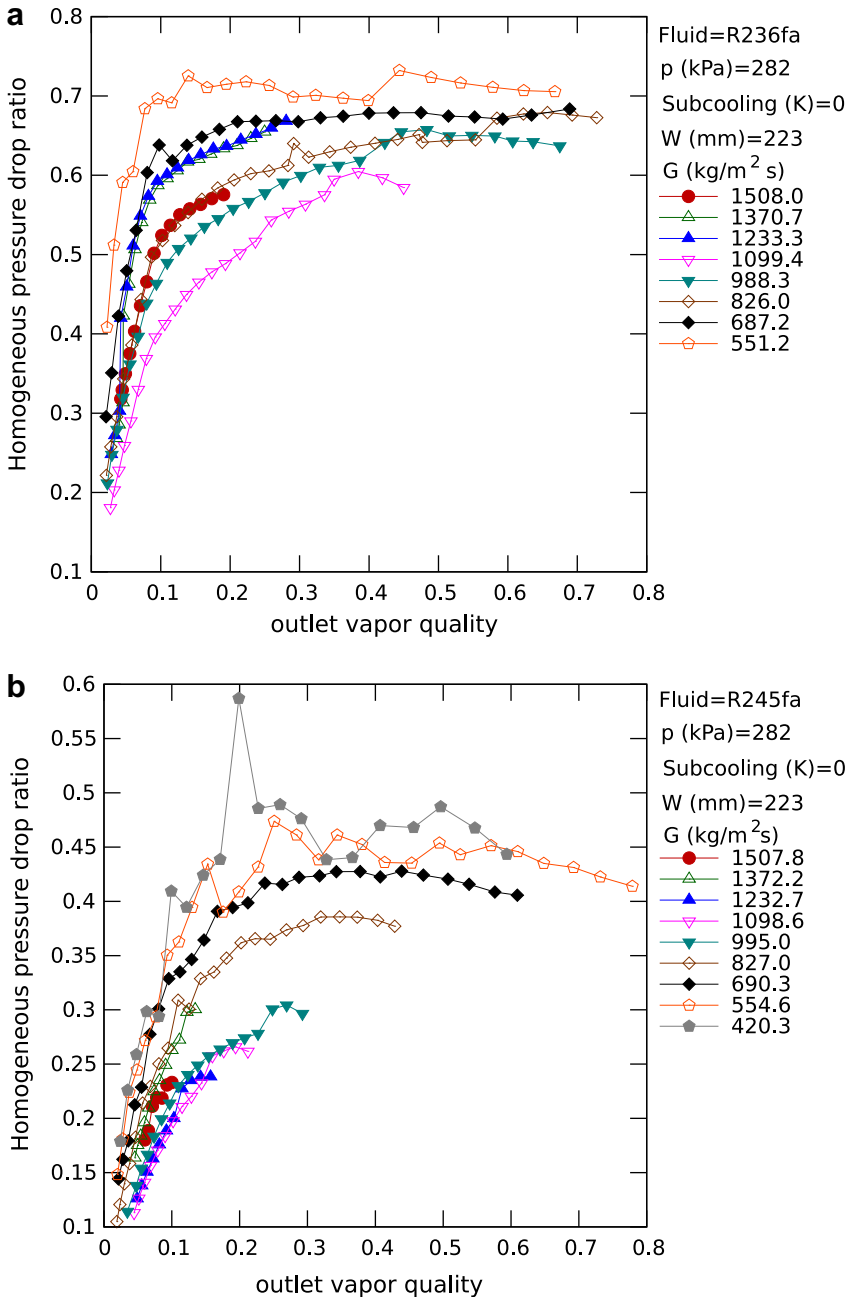

Fig. 10. Microchannel two-phase model pressure drop ratio versus outlet vapour quality for refrigerant R236fa (a) and R245fa (b).

place of Eq. (22) to calculate the two-phase friction factor. However, the Reynolds number of the liquid fraction of the flow can be calculated using the actual velocity of the fluid based on the homogeneous void fraction, so that

$$Re_{\mathrm{l}} = \frac{GD_{\mathrm{h}}(1-x)}{\mu_{\mathrm{L}}(1-\epsilon)} \tag{25}$$

with

$$\epsilon = \frac{1}{1+\frac{1-x}{x}\frac{\rho_{\mathrm{v}}}{\rho_{\mathrm{L}}}}. \tag{26}$$

This "actual" liquid Reynolds number ranges from 970 to 56,357 with 96% of the values above 2000. Thus, although the two-phase Reynolds number given by Eq. (23) suggests the use of a laminar regime expression to calculate the two-phase friction factor, it seems to be physically sounder to use Eq. (22), which corresponds to a turbulent regime.

Fig. 12 shows the total pressure drops predicted with Eq. (20) versus the measured pressure drops for R236fa and R245fa using the values of ξ_{out} determined with the least square method. In fact, 85% of the 896 data points are predicted within ±30%. This analysis shows that the measured total pressure drops vary as G^2 and is linear with x for a large range of mass velocities and vapour qualities, which is characteristic of the homogeneous model. Consequently, this is an additional indication that the homoge-

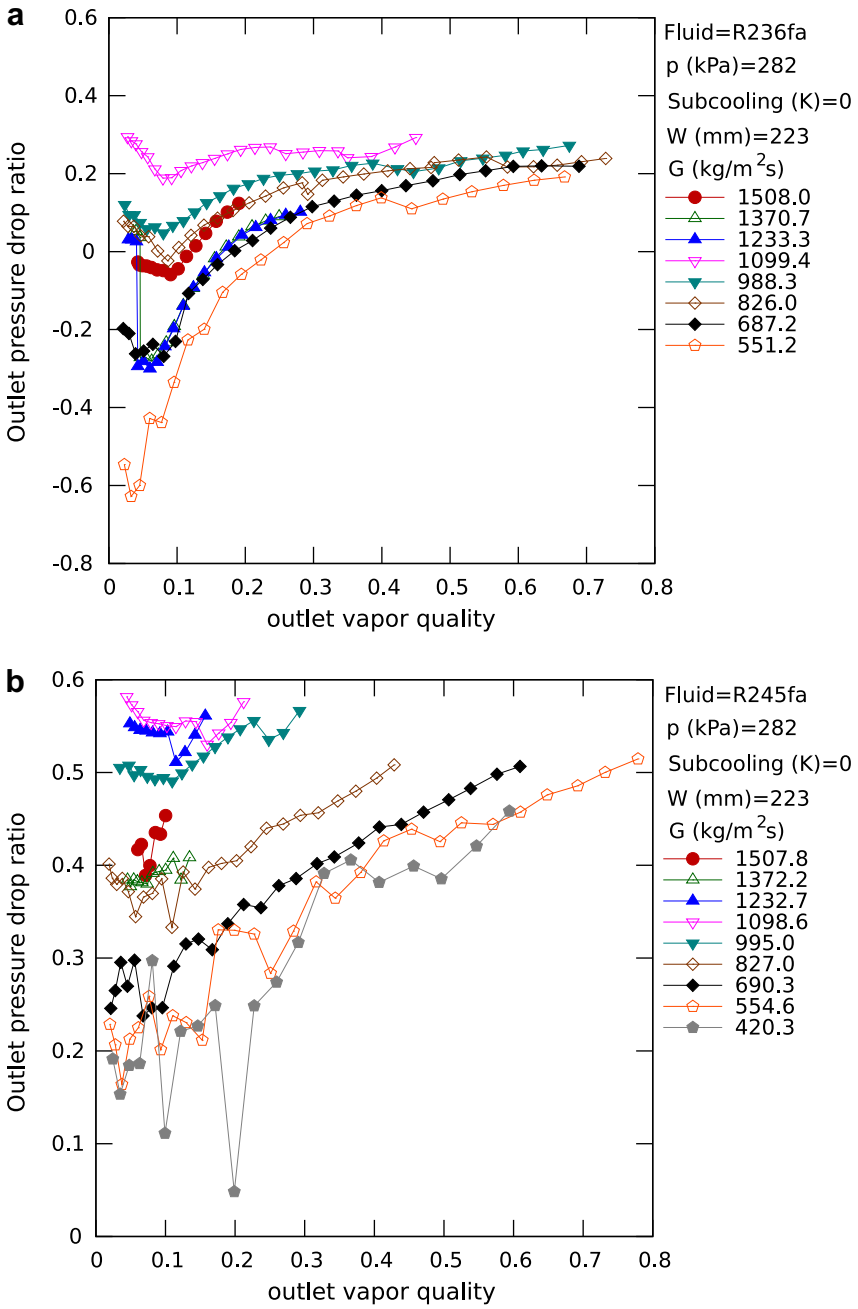

Fig. 11. Outlet pressure drop ratio versus outlet vapour quality for refrigerant R236fa (a) and R245fa (b).

neous model is indeed appropriate to predict microchannel two-phase pressure drops. This analysis also provides a way to predict pressure drops with the present configuration for a future optimization of the design.

8. Conclusions

New experimental critical heat flux results for saturated local conditions (26 data points) have been obtained for R236fa flowing in a silicon multi-microchannel heat sink composed of 67 parallel channels, 223 μm wide, 680 μm high and with 80 μm thick fins separating the channels, 20 mm long, with inlet orifices.

CHF was detected when the difference between the wall and the saturation temperatures was greater than 70 K. The base critical heat flux varied from 112 to 250 W/cm^2 and the wall critical heat flux from 21.9 to 52.2 W/cm^2 for mass velocities between 276 and 992 kg/m^2 s. When increasing the mass velocity, the wall critical heat flux also increased. The inlet saturation temperatures ($20.31 \leqslant T_{sat,in} \leqslant 34.27$ °C) and the inlet subcoolings ($0.4 \leqslant \Delta T_{sub} \leqslant 15.3$ K) were found to have a negligible influence on the wall CHF.

Macro-scale methods [6,10–13] and micro-scale methods (Zhang et al. [14] for water in round microchannels, Qu and Mudawar [15] for water and R113 in rectangular

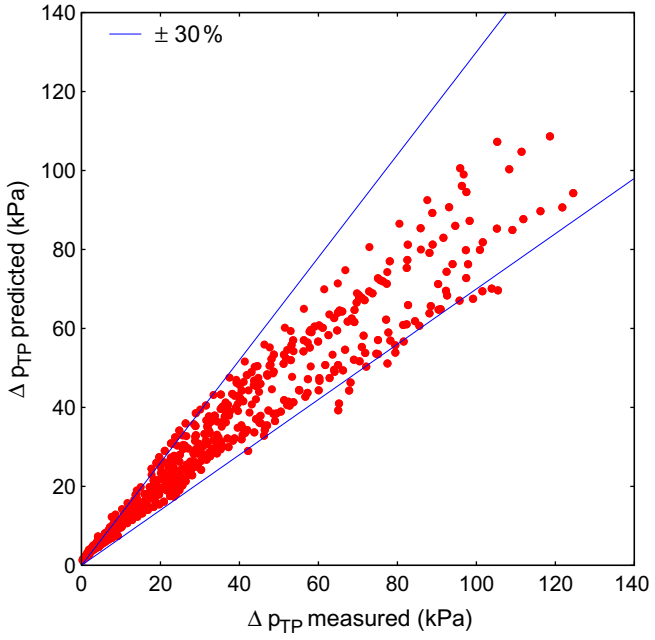

Fig. 12. Total pressure drops predicted with the homogeneous model including inlet and outlet pressure losses versus the measured total pressure drop, for refrigerant R236fa and R245fa.

multi-microchannels, Kuan [17] for water and R123 in multi-microchannels, Wojtan et al. [1] for refrigerants in round microchannels and Revellin and Thome [2], which is a numerical model potentially applicable to any microchannel geometry and fluid) were compared to the database. The correlations developed for rectangular channels tended to overpredict the present CHF data whereas the methods for circular geometries underpredicted them. The best methods were Wojtan et al. [1] correlation and Revellin and Thome [2] model. They both predicted 100% of the experimental CHF results to within ±20% with the heated equivalent diameter taken as the characteristic diameter.

Calculating the critical vapour quality from the CHF, an annular-to-dryout transition is also obtained as a design limit in a diabatic microscale flow pattern map. Beyond this transition, damage from overheating would occur for the device being cooled by the microchannels.

The pressure drop during flow boiling in multi-microchannels was investigated for R236fa and R245fa, showing that R245fa yields higher pressure drops for chip cooling applications, due to its low vapour density. The total pressure drop was shown to increase almost linearly with vapour quality and as the square of the mass velocity, and to decrease with increasing saturation temperature. Furthermore, an analysis of the relative importance of the liquid, two-phase and outlet pressure drops showed that for this channel geometry and at the mass velocity and vapour quality required for a chip cooling application, the pressure drop is mainly controlled by the two-phase flow in the microchannels and not the headers with their orifices. However, the outlet pressure drop is not negligible and can represent up to 30% of the total pressure drop. Furthermore, it was shown that the homogeneous model correctly predicted these pressure drop trends and is recommended to be used together with the inlet and outlet singular pressure drops to predict the total pressure drop in the present multi-microchannel configuration.

Acknowledgements

The authors thank the Swiss Federal Office for Professional Education and Technology (KTI) for sponsoring this work under contract No. 6862.2 DCS-NM and for providing the financial support for Dr. B. Agostini in this project. The authors also wish to recognize the support of the IBM Zürich research center for the construction of the test facility and the fabrication of the test sections. Dr. R. Revellin was supported by the Swiss National Science Foundation (SFN) Grant No. 20111626/1 for his contribution on CHF in this project.

References

[1] L. Wojtan, R. Revellin, J.R. Thome, Investigation of critical heat flux in single, uniformly heated microchannels, Exp. Therm. Fluid Sci. 30 (2006) 765–774.
[2] R. Revellin, J.R. Thome, A theoretical model for the prediction of the critical heat flux in heated microchannels, Int. J. Heat Mass Transfer 51 (2008) 1216–1225.
[3] S.G. Kandlikar, S.G. Li, D. Li, S. Colin, M.R. King, Heat Transfer and Fluid Flow in Minichannels and Microchannels, Elsevier, Amsterdam, 2006.
[4] P.A. Kew, K. Cornwell, Correlations for the prediction of boiling heat transfer in small-diameter channels, Appl. Therm. Eng. 17 (1997) 705–715.
[5] G. Ribatski, L. Wojtan, J.R. Thome, An analysis of experimental data and prediction methods for two-phase frictional pressure drop and flow boiling heat transfer in micro-scale channels, Exp. Therm. Fluid Sci. 31 (2006) 1–19.
[6] Y. Katto, H. Ohno, An improved version of the generalized correlation of critical heat flux for the forced convective boiling in uniformly heated vertical tubes, Int. J. Heat Mass Transfer 27 (9) (1984) 1641–1648.
[7] Y. Katto, S. Yokoya, CHF of forced convection boiling in uniformly heated vertical tubes, experimental study of hp-regime by the use of R12, Int. J. Multiphase Flow 8 (1982) 165–181.
[8] Y. Katto, S. Ashida, CHF in high pressure regime for forced convection boiling in uniformly heated vertical tube of low length-to-diameter-ratio, in: Proceedings of the 7th Int. Heat Transfer Conf., vol. 4, 1982, pp. 291–296.
[9] Y. Katto, S. Yokoya, Critical heat flux of liquid helium (i) in forced convective boiling, Int. J. Multiphase Flow 10 (1984) 401–413.
[10] Y. Katto, General features of chf of forced convection boiling in uniformly heated rectangular channels, Int. J. Heat Mass Transfer 24 (8) (1981) 1413–1419.
[11] M.M. Shah, Improved general correlation for critical heat flux during upflow in uniformly heated vertical tubes, Int. J. Heat Fluid Flow 8 (4) (1987) 326–335.
[12] M.M. Shah, A generalized graphical method for predicting CHF in uniformly heated vertical tubes, Int. J. Heat Mass Transfer 22 (1979) 557–568.
[13] R.W. Bowring, A simple but accurate round tube uniform heat flux, dryout correlation over the pressure range 0.7–17 mn/m^2 (100–2500 psia), in: AEEW-R 789, United Kingdom Atomic Energy Authority, 1972.

[14] W. Zhang, T. Hibiki, K. Mishima, Y. Mi, Correlation for critical heat flux for flow boiling of water in mini-channels, Int. J. Heat Mass Transfer 49 (2006) 1058–1072.
[15] W. Qu, I. Mudawar, Measurement and correlation of critical heat flux in two-phase microchannel heat sinks, Int. J. Heat Mass Transfer 47 (2004) 2045–2059.
[16] M.B. Bowers, I. Mudawar, High flux boiling in low flow rate, low pressure drop mini-channel and micro-channel heat sinks, Int. J. Heat Mass Transfer 37 (1994) 321–332.
[17] W.V. Kuan, Experimental study of flow boiling heat transfer and critical heat flux in microchannels, Ph.D. Thesis, Rochester Institute of Technoloy. Available from: <http://hdl.handle.net/1850/1887> (2006).
[18] A.E. Bergles, S.G. Kandlikar, On the nature of critical heat flux in microchannels, J. Heat Transfer 127 (2005) 101–107.
[19] J.R. Thome, V. Dupont, A.M. Jacobi, Heat transfer model for evaporation in micochannels. Part 1: presentation of the model, Int. J. Heat Mass Transfer 47 (2004) 3375–3385.
[20] R. Revellin, J.R. Thome, New diabatic flow pattern map for evaporating flow in microchannels, in: Proceedings of the 13th Int. Heat Transfer Conf., Sydney, Australia, 2006.
[21] D.J. Pribyl, A. Bar-Cohen, A.E. Bergles, An investigation of critical heat flux and two-phase flow regimes for upward steam and water flow, in: Proceedings of the 5th Int. Conf. in Boiling Heat Transfer, Jamaica, May 4–8, 2003.
[22] A. Ciccitti, C. Lombardi, M. Silvestri, G. Soldaini, R. Zavattarelli, Two-phase cooling experiments – pressure drop, heat transfer and burnout measurements, Energia Nucl. 7 (1960) 407–425.